



## Get Clarity On Generics

Cost-Effective CT & MRI Contrast Agents

 FRESENIUS  
KABI

[WATCH VIDEO](#)

# AJNR

This information is current as  
of August 14, 2025.

## **Automated Determination of the H3 K27-Altered Status in Spinal Cord Diffuse Midline Glioma by Radiomics Based on T2-Weighted MR Images**












Junjie Li, YongZhi Wang, Jinyuan Weng, Liying Qu,  
Minghao Wu, Min Guo, Jun Sun, Geli Hu, Xiaodong Gong,  
Xing Liu, Yunyun Duan, Zhizheng Zhuo, Wenqing Jia and  
Yaou Liu

*AJNR Am J Neuroradiol* 2023, 44 (12) 1464-1470

doi: <https://doi.org/10.3174/ajnr.A8056>

<http://www.ajnr.org/content/44/12/1464>

# Automated Determination of the H3 K27-Altered Status in Spinal Cord Diffuse Midline Glioma by Radiomics Based on T2-Weighted MR Images

 Junjie Li, Yongzhi Wang,  Jinyuan Weng,  Liying Qu, Minghao Wu,  Min Guo,  Jun Sun,  Geli Hu,  Xiaodong Gong,  Xing Liu, Yunyun Duan,  Zhizheng Zhuo,  Wenqing Jia, and  Yaou Liu



## ABSTRACT

**BACKGROUND AND PURPOSE:** Conventional MR imaging is not sufficient to discern the H3 K27-altered status of spinal cord diffuse midline glioma. This study aimed to develop a radiomics-based model based on preoperative T2WI to determine the H3 K27-altered status of spinal cord diffuse midline glioma.

**MATERIALS AND METHODS:** Ninety-seven patients with confirmed spinal cord diffuse midline gliomas were retrospectively recruited and randomly assigned to the training ( $n = 67$ ) and test ( $n = 30$ ) sets. One hundred seven radiomics features were initially extracted from automatically-segmented tumors on T2WI, then 11 features selected by the Pearson correlation coefficient and the Kruskal-Wallis test were used to train and test a logistic regression model for predicting the H3 K27-altered status. Sensitivity analysis was performed using additional random splits of the training and test sets, as well as applying other classifiers for comparison. The performance of the model was evaluated through its accuracy, sensitivity, specificity, and area under the curve. Finally, a prospective set including 28 patients with spinal cord diffuse midline gliomas was used to validate the logistic regression model independently.

**RESULTS:** The logistic regression model accurately predicted the H3 K27-altered status with accuracies of 0.833 and 0.786, sensitivities of 0.813 and 0.750, specificities of 0.857 and 0.833, and areas under the curve of 0.839 and 0.818 in the test and prospective sets, respectively. Sensitivity analysis confirmed the robustness of the model, with predictive accuracies of 0.767–0.833.

**CONCLUSIONS:** Radiomics signatures based on preoperative T2WI could accurately predict the H3 K27-altered status of spinal cord diffuse midline glioma, providing potential benefits for clinical management.

**ABBREVIATIONS:** AUC = area under the curve; CE = contrast-enhanced; DMG = diffuse midline glioma; HR = hazard ratio; LR = logistic regression; NPV = negative predictive value; OS = overall survival; PPV = positive predictive value; SC-DMG = spinal cord diffuse midline glioma; WHO = World Health Organization

Diffuse midline glioma (DMG), which occurs in both children and young adults, is a rare type of glioma first recognized as a new entity in the 2016 World Health Organization (WHO) Classification of CNS Tumors as DMG H3 K27M-mutant. Recently,

it has been renamed DMG H3 K27-altered status in the 2021 WHO Classification.<sup>1–4</sup> Previous evidence demonstrated that H3 K27-altered was a poor prognostic biomarker for DMG, while a recent clinical trial showed that GD2-directed chimeric antigen receptor T-cell therapy had a promising value in reducing tumor volume of DMG H3 K27-altered tumors.<sup>3,5–11</sup>

Currently, the criterion standard techniques to accurately determine the H3 K27-altered status rely on gene sequencing or immunohistochemistry through invasive biopsy or surgical resection.<sup>12</sup> Tissue sampling bias due to intertumoral heterogeneity may reduce the sensitivity and accuracy of H3 K27-altered status determination. Therefore, a noninvasive method using whole-tumor information is warranted to accurately predict the H3 K27-altered status preoperatively.

MR imaging can provide various morphologic and physiologic features to comprehensively characterize glioma heterogeneity.<sup>13</sup> Recently, radiomics based on medical images has become a promising tool for noninvasively assessing the molecular genotypes of gliomas in several studies, providing potential benefits

Received May 8, 2023; accepted after revision October 8.

From the Departments of Radiology (J.L., L.Q., M.W., M.G., J.S., Y.D., Z.Z., Y.L.), Neurosurgery (Y.W., W.J.), and Pathology (X.L.), Beijing Tiantan Hospital, Capital Medical University, Beijing, People's Republic of China; Department of Medical Imaging Products (J.W., X.G.), Neusoft, Group Ltd, Shenyang, People's Republic of China; and Clinical and Technical Support (G.H.), Philips Healthcare, Beijing, People's Republic of China.

J. Li, Y. Wang, and J. Went are first authors who contributed equally to this work. Z. Zhuo, W. Jia, and Y. Liu are senior authors who contributed equally to this work. This work was supported by the Beijing Municipal Natural Science Foundation for Distinguished Young Scholars (No. JQ20035), the Capital Health Development Research Project (No. 2022-1-2042), and the Radiographic Standard Database Construction Project (NO. YXFSC2022JJS004).

Please address correspondence to Yaou Liu, MD, PhD, No.119, the West Southern 4th Ring Rd, Fengtai District, Beijing, 100070, China; e-mail: liuyaou@bjtth.org

 Indicates article with online supplemental data.

<http://dx.doi.org/10.3174/ajnr.A8056>

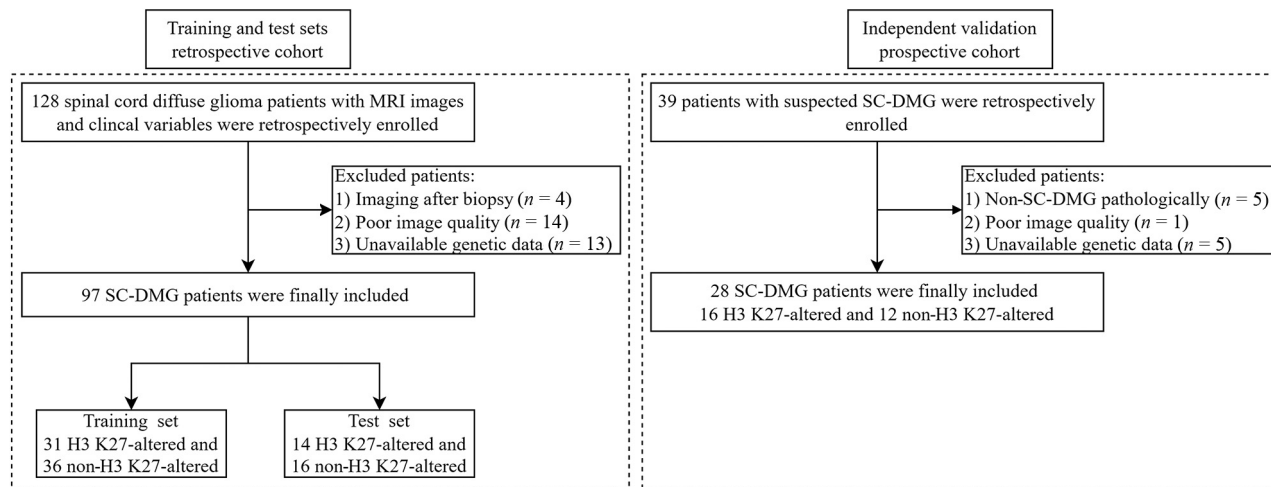


**FIG 1.** Flowchart of the included patients in this study.

for personalized and effective treatment plans.<sup>14,15</sup> Several studies have efficiently predicted the H3 K27-altered status by using radiomics in diffuse midline gliomas in the brainstem.<sup>16,17</sup> However, few studies have focused on spinal cord diffuse midline glioma (SC-DMG) due to its rarity. Conventional features such as hemorrhage and syringohydromyelia appear to have limited predictive value for SC-DMG H3 K27-altered status.<sup>18,19</sup> Developing an accurate, accessible, robust, and noninvasive radiomics approach for detecting the H3 K27-altered status in SC-DMG remains clinically feasible. This study aimed to predict the H3 K27-altered status of SC-DMG by using radiomics from retrospective and prospective cohorts based on T2WI.

## MATERIALS AND METHODS

### Study Design and Patients

This study was approved by the institutional review board of Beijing Tiantan Hospital, Capital Medical University, and written informed consent was obtained from all patients or their legal guardians.

A total of 128 patients with histopathologic diagnosis of diffuse glioma in the spinal cord from December 2013 to October 2019 were retrospectively enrolled. A total of 97 patients was finally included on the basis of the following inclusion criteria: 1) preoperative sagittal T2WI scans with adequate image quality; 2) available H3 K27-altered status. Exclusion criteria were the following: 1) a history of biopsy or an operation before MR imaging; 2) poor image quality (eg, obvious motion artifacts, distortion, and signal loss); 3) unknown H3 K27-altered status (Fig 1). From November 2019 to June 2022, thirty-nine patients with suspected SC-DMG were prospectively recruited for independent validation. Inclusion criteria were the following: 1) SC-DMG pathologically confirmed by biopsy or surgical resection; 2) no treatment history before MR imaging; 3) available H3 K27-altered status. Exclusion criteria were the following: 1) pathologic confirmation of other diseases; 2) poor image quality; 3) unknown H3 K27-altered status (Fig 1). MR images, including sagittal T2WI, T1WI, and contrast-enhanced (CE) CE-T1WI, as well as clinical variables, including patient demographics, treatment information, survival status, and detailed pathologic data, were obtained.

After applying the inclusion and exclusion criteria, the final study cohort consisted of 97 patients in the retrospective cohort who were divided into a training set ( $n = 67$ , including 31 H3 K27-altered and 36 non-H3 K27-altered cases) and a test set ( $n = 30$ , including 14 H3 K27-altered and 16 non-H3 K27-altered cases) to build a H3 K27-altered predictive model. Then, an independent prospective cohort of 28 patients, including 16 H3 K27-altered and 12 non-H3 K27-altered cases, was enrolled to validate the predictive model. Further survival analysis was performed to confirm the clinical prognostic prediction value of the H3 K27-altered status of SC-DMG.

### Neuropathology Analysis

All tumor histopathologic grading was evaluated following the 2016 WHO Classification using formalin-fixed/paraffin-embedded samples with H&E staining. The H3 K27-altered (H3 K27M mutation) status was assessed through immunohistochemistry using the corresponding specific antibody (ABE419; MilliporeSigma; 1:800).

### MR Imaging Acquisition

Spinal cord MR images were acquired using 6 MR imaging scanners: SIGNA HDe and Discovery 750 (GE Healthcare), Ingenia CX (Philips Healthcare), and Verio, Magnetom Trio, and Magnetom Prisma (Siemens). MR imaging protocols (T2WI, T1WI, and CE-T1WI) for intramedullary spinal cord lesions and parameters are found in the Online Supplemental Table 1.

### MR Image Preprocessing

For all patients whose images were used with tumor segmentation, T2WI was first corrected for N4 bias using the SimpleITK python package (<https://pypi.org/project/SimpleITK/>). The image signal intensities were normalized by subtracting the mean value and dividing by the SD of the signal intensity.

### Assessment of MR Imaging Characteristics

Conventional MR imaging features, including tumor location, length, edema, cystic/necrosis, contrast-enhancement status, and syringohydromyelia, were assessed by a senior neuroradiologist (Y.D., with >13 years of experience in neuroradiology) and a

junior neuroradiologist (M.G., with >4 years of experience in neuroradiology) who were blinded to clinicopathologic data. Because there were high interrater agreements (K-values ranged from 0.71 to 1) on the MR imaging assessments, we presented the MR imaging assessments by the senior neuroradiologist in the main text and provided those by the junior neuroradiologist in the Online Supplemental Table 2. Tumor location was classified as cervical, cervicothoracic, thoracic, thoracolumbar, or lumbar vertebral, on the basis of the area involving the main component of the tumor. Tumor length was defined as the number of tumor-involved vertebrae. Edema was reflected by greater signal intensity than in the tumor noncontrast portion, lower signal intensity than in the CSF, and unclear boundaries on the T2WI.<sup>20</sup> The presentation of cystic or necrosis was well-defined as high-T2WI and low-T1WI signals essentially matching the CSF signals and nonenhanced wall. Compared with T1WI, the tumor CE pattern was classified as no enhancement (including mild enhancement) and obvious enhancement on CE-T1WI. Syringohydromyelia was defined as cystic dilation of the central portion of the spinal cord on T2WI without wall enhancement.<sup>20,21</sup>

### **Radiomics Feature Extraction**

Tumor segmentation on T2WI was automatically performed by a deep learning model developed by our research team (the mean Dice score of tumor segmentation was 0.852) and visually checked by a senior neuroradiologist (Y.D.) (8 of 97 patients in the retrospective cohort required additional manual review and correction).<sup>22,23</sup> Radiomics features of tumors were then extracted using Feature Analysis Explorer (FAE, Version 0.5.2; <https://github.com/salan668/FAE>) software. One hundred seven original radiomics features, including 14 shape-based features, 18 first-order features, 24 gray-level co-occurrence matrix features, 14 gray-level dependence matrix features, 16 gray-level run length matrix features, 16 gray-level size zone matrix features, and 5 neighboring gray tone difference matrix features, from T2WI were extracted.

### **Feature Processing and Selection**

Using FAE, we adopted an up-sampling strategy to balance the H3 K27-altered and non-H3 K27-altered cases in the training set. Z score transformation was used for feature normalization. The Pearson correlation coefficient assessment was performed for feature-dimension reduction by randomly removing one of the paired features with high similarity (Pearson correlation coefficient > 0.99), followed by the Kruskal-Wallis method for selection of the optimal features.

### **Model Development**

Logistic regression (LR) was used to determine the H3 K27-altered status by using the selected radiomics features. Five-fold cross-validation was performed for model parameter optimization in the training set. Then, we evaluated the performance of the model in the test set, by determining the classification accuracy, sensitivity, specificity, positive predictive value (PPV), negative predictive value (NPV), and area under the curve (AUC).

### **Sensitivity Analysis**

Sensitivity analysis was performed to support the main findings using the LR radiomics model in the test set: 1) We compared the

other 2 conventional MR imaging radiomic features, T1WI and CE-T1WI, to assess whether this additional information could improve the performance of the model. 2) To exclude potential bias in separating the training and test sets, we repeated the pipeline with 4 additional random splits of the training and test sets. 3) We included 4 classifiers, including support vector machine, least absolute shrinkage, and selection operator regression; linear discriminant analysis; and the Gaussian process for comparison to support the performance of the LR model. 4) We evaluated the predictive performance of combined original radiomics features and their variant features in comparison with the original radiomic features.

### **Survival Analysis**

The overall survival (OS) of a subset of 79 patients was finally available, including 33 H3 K27-altered and 46 non-H3 K27-altered cases. The therapeutic regimen (eg, extent of tumor resection and postoperative treatment) was obtained from the medical records and follow-up visits. The extent of tumor resection was classified as total, subtotal, partial resection, or biopsy on the basis of medical records. Postoperative treatment included chemotherapy and radiation therapy.

### **Statistical Analysis**

Statistical analysis was performed with SPSS (SPSS for Windows, Version 26.0; IBM) and the R statistical and computing software (Version 4.2.1; <http://www.r-project.org/>). Categorical variables were expressed as frequency and compared using the  $\chi^2$  test or Fisher exact test. Continuous variables were expressed as mean (SD) and compared using the Student *t* test or Mann-Whitney *U* test. *P* < .05 was considered statistically significant. Classification accuracy, sensitivity, specificity, PPV, NPV, and AUC were calculated to evaluate the performance of the model. OS was estimated by Kaplan-Meier survival curve analysis and the logrank test using the survminer package in R (<https://cran.r-project.org/web/packages/survminer/index.html>). Using the coxph package (<https://www.rdocumentation.org/packages/survival/versions/3.5-7/topics/coxph>), the univariate and multivariate Cox proportional hazards models were used to evaluate the model's performance with the WHO grade that integrating the H3 K27-altered status and histologic grade, and other clinical variables in predicting OS. *P* < .05 was considered statistically significant.

## **RESULTS**

### **Demographic and MR Imaging Characteristics**

Detailed demographic and MR imaging characteristics are shown in Online Supplemental Data. In the retrospective cohort, no differences were observed between the H3 K27-altered and non-H3 K27-altered groups in age, sex, tumor location, tumor length, and tumor enhancement. As for MR imaging characteristics, non-H3 K27-altered SC-DMG cases exhibited higher rates of edema, cystic/necrosis, and syringohydromyelia compared with the H3 K27-altered group (*P* < .05). There were no significant differences in terms of demographic and MR imaging features in the prospective set.

**Prediction of H3 K27-Altered Status by Radiomics.** Figure 2 shows 6 representative cases (4 correctly predicted cases and 2 wrongly predicted cases) and their corresponding predicted probability



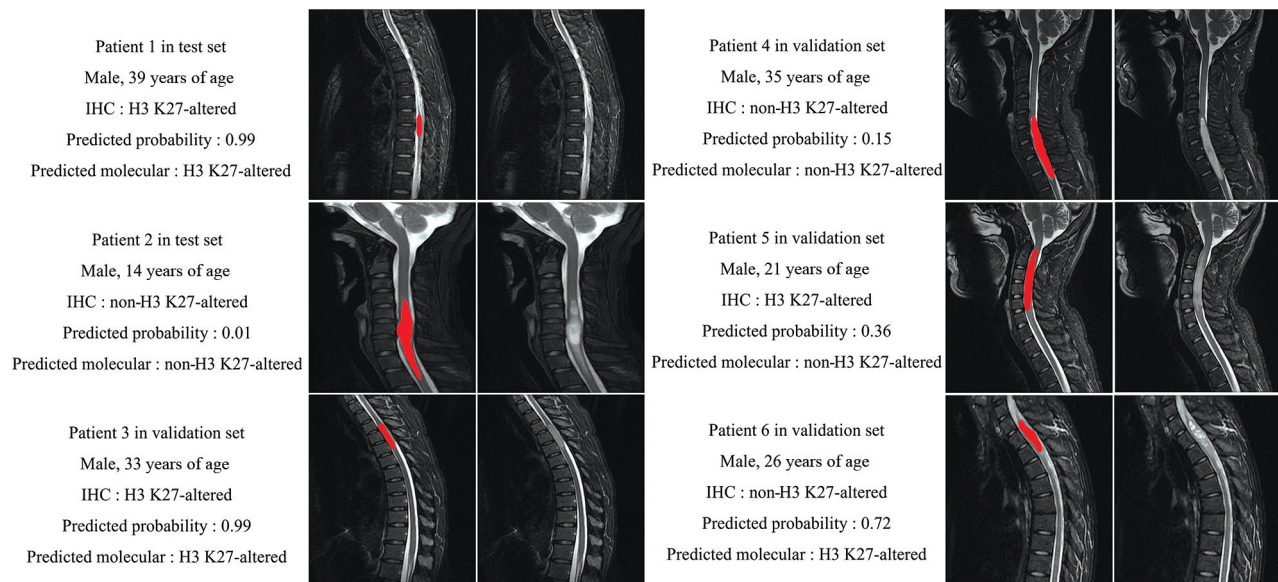


**FIG 2.** Six representative patients with SC-DMG in the test and validation sets, including 4 correctly predicted cases and 2 wrongly predicted cases. Immunohistochemistry (IHC) showed the H3 K27-altered status of each patient. The predicted probability and predicted molecular status were calculated by using the LR model. *Red overlay* indicates the tumor segmentation.

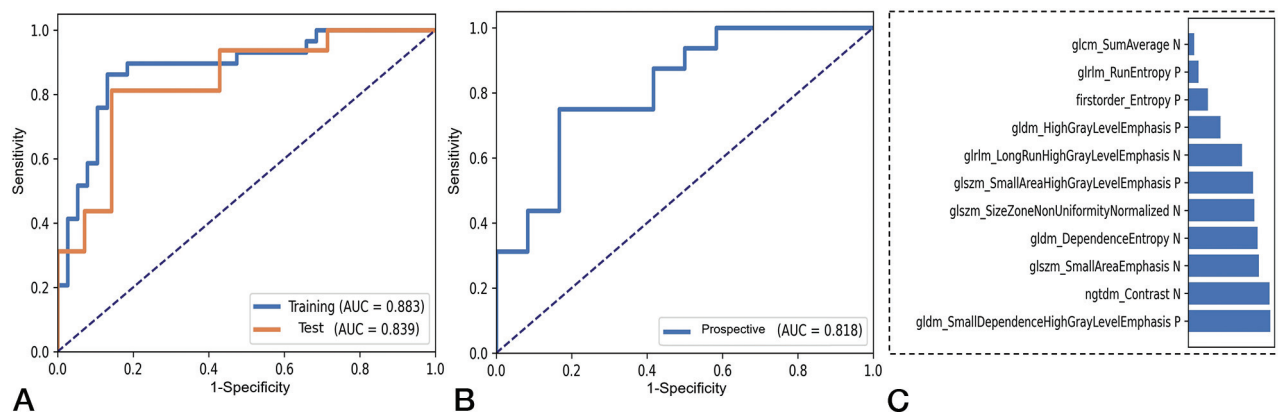


**FIG 3.** A and B, Receiver operating characteristic curve analysis of the LR model for predicting the H3 K27-altered status in the retrospective cohort (A) and in the independent prospective cohort (B). C, The 11 selected radiomics features with the highest average importance.

calculated by the cutoff value of the LR model. The LR predictive model based on 11 radiomics features achieved an accuracy of 0.833, a sensitivity of 0.813, a specificity of 0.857, a PPV of 0.867, a NPV of 0.800, and an AUC of 0.839 in the test set (Fig 3A and Online Supplemental Data). In the independent prospective set, the predictive model achieved an accuracy of 0.786, a sensitivity of 0.750, a specificity of 0.833, a PPV of 0.857, a NPV of 0.714, and an AUC of 0.818 (Fig 3B and Online Supplemental Data). The 11 important radiomics features are shown in Fig 3C and the Online Supplemental Table 3.

### Sensitivity Analysis

The predictive performance of other conventional models (T1WI and CE-T1WI) was lower than that of the LR model (accuracy range of 0.553–0.700) (Online Supplemental Data and Online Supplemental Table 4). Another 4 random splits of the training and test sets demonstrated comparable predictive abilities (accuracy

range of 0.767–0.833) (Online Supplemental Data). Other classifiers had comparable performance to predict SC-DMG H3 K27-altered status with accuracies ranging from 0.767 to 0.800 (Online Supplemental Data). Different age and field strength subgroups had comparable performance, with accuracies ranging from 0.750 to 0.818 (Online Supplemental Table 5). The combined original radiomics features and their variant features had comparable performance with an accuracy of 0.821 in the test set (Online Supplemental Table 6).

### Survival Analysis

Kaplan-Meier curve analysis revealed that patients with SC-DMG H3 K27-altered status had worse OS than those with non-H3 K27-altered tumors (logrank test,  $P < .001$ ) (Fig 4), with a median OS in non-H3 K27-altered cases of 40.7 (SD, 26.4) months versus 24.3 (SD, 17.6) months in H3 K27-altered cases (Online Supplemental Table 7). Univariate Cox regression analysis showed

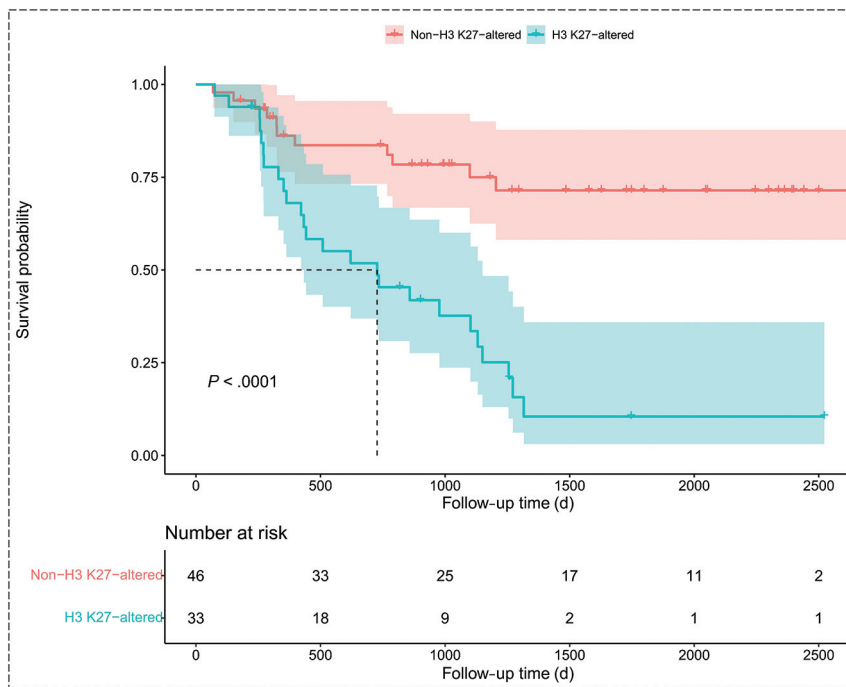


**FIG 4.** Kaplan-Meier survival curves for H3 K27-altered and non-H3 K27-altered SC-DMG.

that sex, age, syringohydromyelia, extent of resection, and WHO grades were risk factors for OS, with hazard ratios (HRs) of 0.44 (95% CI, 0.23–0.86;  $P = .016$ ), 1.02 (95% CI, 1.00–1.05;  $P = .010$ ), 0.14 (95% CI, 0.03–0.592;  $P = .007$ ), 1.93 (95% CI, 1.21–3.09;  $P = .006$ ), and 3.19 (95% CI, 1.97–5.16;  $P = .001$ ), respectively. Multivariate Cox regression analysis showed the WHO grade as an independent risk factor for OS (HR = 4.48, 95% CI, 1.90–10.59;  $P = .001$ ). We also analyzed the H3 K27-altered status and histologic grade factors by Cox analysis (Online Supplemental Tables 8 and 9).

## DISCUSSION

In the current study, we constructed an LR predictive model on the basis of T2WI-based radiomics features in SC-DMG for preoperatively and accurately predicting the H3 K27-altered status. This model using only T2WI showed a robust performance in predicting the H3 K27-altered status, with an accuracy of 0.833 in the test set and 0.767 in the independent prospective cohort.

Age and sex showed no differences between H3 K27-altered and non-H3 K27-altered SC-DMG, which corroborated previous reports.<sup>9,18,19,24</sup> The conventional MR imaging presentations of H3 K27-altered or non-H3 K27-altered SC-DMG are still unclear due to limited sample sizes ( $n < 25$ ) in most previous studies.<sup>3,10,25–29</sup> Compared with non-H3 K27-altered SC-DMG, only a few studies reporting H3 K27-altered SC-DMG showed more hemorrhage and less syringohydromyelia.<sup>18,19</sup> In this study, conventional MR imaging presentations, including edema, cyst/necrosis, and syringohydromyelia, showed differences between H3 K27-altered SC-DMG and non-H3 K27-altered SC-DMG in the retrospective cohort, but they had an insufficient predictive ability with a low accuracy of 53.5%. In addition, no difference in

these features was observed in the prospective validation cohort. These findings indicated that the conventional MR imaging features may have limited value for the determination of the H3 K27-altered SC-DMG. Further studies with large samples are warranted to confirm the current findings and identify specific MR imaging features of H3 K27-altered SC-DMG.

Previous studies have focused on predicting the H3 K27-altered status in brain gliomas by MR imaging.<sup>16,17,25,30,31</sup> Our study predicted the H3 K27-altered status of SC-DMG using MR imaging-based radiomics, which demonstrated superior performance compared with conventional features. The predictive model had an accuracy of 0.833 and an AUC of 0.839 in the test set. This finding was further supported by an accuracy of 0.786 and an AUC of 0.818 in an independent prospective set. The high diagnostic performance based on 11 radiomics features extracted from T2WI

associated with the distribution of pixel intensity, the relative position of the various gray levels, and the description of patterns or the spatial distribution of voxel intensities may help determine SC-DMG H3 K27-altered status. These findings showed that T2WI may be the most helpful imaging technique, because it could clearly depict high-signal lesions, swelling, cavities, and edema features, while, presumably, enhancement characteristics may play little role, as indicated by the lower value of CE-T1WI in the determination of H3K27-altered SC-DMG.

Sensitivity analysis demonstrated the robustness of the LR predictive model. The primary results (accuracy of 0.833 in the test set) were better than those in other models using conventional MR imaging features and radiomics features from T1WI and CE-T1WI (accuracies ranging from 0.533 to 0.700 in the test set). Comparable predictive performance (accuracies ranging from 0.767 to 0.833) using random splits of the training and test sets indicated the absence of sample bias for the training and test splits in the primary findings. The predictive performance of other classifiers (accuracies ranging from 0.767 to 0.800) was comparable with that of our LR radiomics model, which indicated little model selection bias and the robustness of the MR imaging features for predicting H3 K27-altered status. Subgroup analyses in children and adults (accuracies ranging from 0.750 to 0.773) and the analysis of field strength (accuracies ranging from 0.737 to 0.818) demonstrated its generalizability for clinical practice. The combined original radiomics features and their variant features achieved a predictive accuracy of 0.821 in the test set, with performance comparable with that of the main results.

H3 K27-altered status in SC-DMG initiates tumorigenesis by affecting epigenetic regulation, transcriptional changes, and oncogenic activation.<sup>32</sup> In the current study, a relatively large sample size of 79 SC-DMG cases with grades 2–4 was included, and SC-

DMG H3 K27-altered status was identified as a poor prognostic factor, consistent with several previous studies confirming the deleterious role of H3 K27-altered status in SC-DMG.<sup>10,19</sup> However, some studies have shown that patients with SC-DMG with H3 K27-altered status have a better prognosis.<sup>7,9</sup> This discrepancy may be explained by potential sample selection bias in their smaller samples ( $n < 30$ ) and the effects of other unreported genetic alterations in addition to the H3 K27-altered status.<sup>24</sup>

The present study had several limitations. First, all patients were from a single center in this study. More extensive studies and external validations are required in prospective and multi-institutional settings. Second, the main variants of histone H3, the H3.1 (HIST1H3B/C) and H3.3 (H3F3A) mutations, which represent distinct subgroups with different prognostic and phenotypic patterns in glioma, were not analyzed.<sup>33</sup> Only H3 K27M mutation and wild-type status were assessed in the current study, and the H3 K27-altered status of some patients before 2016 was analyzed according to the 2016 WHO Classification, which may have introduced a potential selection bias. Third, the pathophysiologic processes underlying T2WI-based radiomics features and their mechanisms need to be determined for reasonable interpretation. Last, the reproducibility of the radiomics method and the heterogeneity across various MR imaging devices and sequences, such as spectral presaturation with inversion recovery (SPIR), STIR, and Dixon, should be considered.

## CONCLUSIONS

The radiomics signatures based on T2WI could noninvasively predict H3 K27-altered status of SC-DMG. These could serve as a noninvasive tool providing reliable molecular information to aid in the clinical treatment of SC-DMG.

## ACKNOWLEDGMENT

We acknowledge all the colleagues who helped with the patient recruitment and MR imaging.

Disclosure forms provided by the authors are available with the full text and PDF of this article at [www.ajnr.org](http://www.ajnr.org).

## REFERENCES

- Fakhreddine MH, Mahajan A, Penas-Prado M, et al. Treatment, prognostic factors, and outcomes in spinal cord astrocytomas. *Neuro Oncol* 2013;15:406–12 [CrossRef Medline](#)
- Abd-El-Barr MM, Huang KT, Moses ZB, et al. Recent advances in intradural spinal tumors. *Neuro Oncol* 2018;20:729–42 [CrossRef Medline](#)
- Meyronet D, Esteban-Mader M, Bonnet C, et al. Characteristics of H3 K27M-mutant gliomas in adults. *Neuro Oncol* 2017;19:1127–34 [CrossRef Medline](#)
- Louis DN, Perry A, Wesseling P, et al. The 2021 WHO Classification of Tumors of the Central Nervous System: a summary. *Neuro Oncol* 2021;23:1231–51 [CrossRef Medline](#)
- Louis DN, Giannini C, Capper D, et al. cIMPACT-NOW update 2: diagnostic clarifications for diffuse midline glioma, H3 K27M-mutant and diffuse astrocytoma/anaplastic astrocytoma, IDH-mutant. *Acta Neuropathol* 2018;135:639–42 [CrossRef Medline](#)
- Aquilanti E, Miller J, Santagata S, et al. Updates in prognostic markers for gliomas. *Neuro Oncol* 2018;20:vii17–26 [CrossRef Medline](#)
- Yi S, Choi S, Shin DA, et al. Impact of H3.3 K27M mutation on prognosis and survival of grade IV spinal cord glioma on the basis of new 2016 World Health Organization Classification of the Central Nervous System. *Neurosurgery* 2019;84:1072–81 [CrossRef Medline](#)
- Chai RC, Zhang YW, Liu YQ, et al. The molecular characteristics of spinal cord gliomas with or without H3 K27M mutation. *Acta Neuropathol Commun* 2020;8:40 [CrossRef Medline](#)
- Akinduro OO, Garcia DP, Higgins DM, et al. A multicenter analysis of the prognostic value of histone H3 K27M mutation in adult high-grade spinal glioma. *J Neurosurg Spine* 2021;35:834–43 [CrossRef Medline](#)
- Karremann M, Gielen GH, Hoffmann M, et al. Diffuse high-grade gliomas with H3 K27M mutations carry a dismal prognosis independent of tumor location. *Neuro Oncol* 2018;20:123–31 [CrossRef Medline](#)
- Majzner RG, Ramakrishna S, Yeom KW, et al. GD2-CAR T cell therapy for H3K27M-mutated diffuse midline gliomas. *Nature* 2022;603:934–41 [CrossRef Medline](#)
- Gielen GH, Gessi M, Buttarelli FR, et al. Genetic analysis of diffuse high-grade astrocytomas in infancy defines a novel molecular entity. *Brain Pathol* 2015;25:409–17 [CrossRef Medline](#)
- Thust SC, Heiland S, Falini A, et al. Glioma imaging in Europe: a survey of 220 centres and recommendations for best clinical practice. *Eur Radiol* 2018;28:3306–17 [CrossRef Medline](#)
- Rudie JD, Rauschecker AM, Bryan RN, et al. Emerging applications of artificial intelligence in neuro-oncology. *Radiology* 2019;290:607–18 [CrossRef Medline](#)
- Bhandari AP, Liong R, Koppen J, et al. Noninvasive determination of IDH and 1p19q status of lower-grade gliomas using MRI radiomics: a systematic review. *AJNR Am J Neuroradiol* 2021;42:94–101 [CrossRef Medline](#)
- Su X, Chen N, Sun H, et al. Automated machine learning based on radiomics features predicts H3 K27M mutation in midline gliomas of the brain. *Neuro Oncol* 2020;22:393–401 [CrossRef Medline](#)
- Zhuo Z, Qu L, Zhang P, et al. Prediction of H3K27M-mutant brainstem glioma by amide proton transfer-weighted imaging and its derived radiomics. *Eur J Nucl Med Mol Imaging* 2021;48:4426–36 [CrossRef Medline](#)
- Jung JS, Choi YS, Ahn SS, et al. Differentiation between spinal cord diffuse midline glioma with histone H3 K27M mutation and wild type: comparative magnetic resonance imaging. *Neuroradiology* 2019;61:313–22 [CrossRef Medline](#)
- Cheng L, Wang L, Yao Q, et al. Clinoradiological characteristics of primary spinal cord H3 K27M-mutant diffuse midline glioma. *J Neurosurg Spine* 2021;36:1–12 [CrossRef Medline](#)
- Kim DH, Kim JH, Choi SH, et al. Differentiation between intramedullary spinal ependymoma and astrocytoma: comparative MRI analysis. *Clin Radiol* 2014;69:29–35 [CrossRef Medline](#)
- Timponi VM, Patel SH. MRI of a syrinx: is contrast material always necessary? *AJR Am J Roentgenol* 2015;204:1082–85 [CrossRef Medline](#)
- Lemay A, Gros C, Zhuo Z, et al. Automatic multiclass intramedullary spinal cord tumor segmentation on MRI with deep learning. *Neuroimage Clin* 2021;31:102766 [CrossRef Medline](#)
- Sun T, Wang Y, Liu X, et al. Deep learning based on preoperative magnetic resonance (MR) images improves the predictive power of survival models in primary spinal cord astrocytomas. *Neuro Oncol* 2023;25:1157–65 [CrossRef Medline](#)
- Wang L, Li Z, Zhang M, et al. H3 K27M-mutant diffuse midline gliomas in different anatomical locations. *Hum Pathol* 2018;78:89–96 [CrossRef Medline](#)
- Piccardo A, Tortora D, Mascelli S, et al. Advanced MR imaging and 18F-DOPA PET characteristics of H3K27M-mutant and wild-type pediatric diffuse midline gliomas. *Eur J Nucl Med Mol Imaging* 2019;46:1685–94 [CrossRef Medline](#)
- Qiu T, Chanchotisatien A, Qin Z, et al. Imaging characteristics of adult H3 K27M-mutant gliomas. *J Neurosurg* 2019;133:1662–70 [CrossRef Medline](#)
- Schulte JD, Buerki RA, Lapointe S, et al. Clinical, radiologic, and genetic characteristics of histone H3 K27M-mutant diffuse midline gliomas in adults. *Neurooncol Adv* 2020;2:vdaa142 [CrossRef Medline](#)

28. Schreck KC, Ranjan S, Skorupan N, et al. **Incidence and clinicopathologic features of H3 K27M mutations in adults with radiographically-determined midline gliomas.** *J Neurooncol* 2019;143:87–93 [CrossRef Medline](#)
29. Wang YZ, Zhang YW, Liu WH, et al. **Spinal cord diffuse midline gliomas with H3 K27m-mutant: clinicopathological features and prognosis.** *Neurosurgery* 2021;89:300–07 [CrossRef Medline](#)
30. Kandemirli SG, Kocak B, Naganawa S, et al. **Machine learning-based multiparametric magnetic resonance imaging radiomics for prediction of H3K27M mutation in midline gliomas.** *World Neurosurg* 2021;151:e78–85 [CrossRef Medline](#)
31. Pan CC, Liu J, Tang J, et al. **A machine learning-based prediction model of H3K27M mutations in brainstem gliomas using conventional MRI and clinical features.** *Radiother Oncol* 2019;130:172–79 [CrossRef Medline](#)
32. Nagaraja S, Quezada MA, Gillespie SM, et al. **Histone variant and cell context determine H3K27M reprogramming of the enhancer landscape and oncogenic state.** *Mol Cell* 2019;76:965–80.e12 [CrossRef Medline](#)
33. Castel D, Philippe C, Calmon R, et al. **Histone H3F3A and HIST1H3B K27M mutations define two subgroups of diffuse intrinsic pontine gliomas with different prognosis and phenotypes.** *Acta Neuropathol* 2015;130:815–27 [CrossRef Medline](#)